



**HAL**  
open science

## Ultra-small Platinum-based coordination nanoparticles for radiotherapy

Riya George, Lucile Fétiveau, Erika Porcel, Farah Savina, Charles Bosson,  
Diana Dragoë, Hynd Remita, Sandrine Lacombe, Laure Catala

► **To cite this version:**

Riya George, Lucile Fétiveau, Erika Porcel, Farah Savina, Charles Bosson, et al.. Ultra-small Platinum-based coordination nanoparticles for radiotherapy. *Materials Advances*, 2023, 4 (21), pp.5314-5323. 10.1039/D3MA00516J . hal-04303895

**HAL Id: hal-04303895**

**<https://cnrs.hal.science/hal-04303895>**

Submitted on 23 Nov 2023

**HAL** is a multi-disciplinary open access archive for the deposit and dissemination of scientific research documents, whether they are published or not. The documents may come from teaching and research institutions in France or abroad, or from public or private research centers.

L'archive ouverte pluridisciplinaire **HAL**, est destinée au dépôt et à la diffusion de documents scientifiques de niveau recherche, publiés ou non, émanant des établissements d'enseignement et de recherche français ou étrangers, des laboratoires publics ou privés.

## ARTICLE

## Ultra-small Platinum-based coordination nanoparticles for radiotherapy

Riya George,<sup>\*a</sup> Lucile Fétiveau,<sup>a</sup> Erika Porcel,<sup>\*b</sup> Farah Savina,<sup>b</sup> Charles Bosson,<sup>b</sup> Diana Dragoie,<sup>a</sup> Hynd Remita,<sup>c</sup> Sandrine Lacombe,<sup>b</sup> and Laure Catala<sup>\*a</sup>

Received 00th January 20xx,  
Accepted 00th January 20xx

DOI: 10.1039/x0xx00000x

Radiation therapy is an effective and localised method of cancer treatment and its efficacy is considerably improved by using radiosensitizing agents. Nanoparticles containing high atomic number (Z) elements have emerged as an appealing class of sensitizers/enhancers. This work reports the first example of radiosensitizers based on ultrasmall platinum (Pt)-polycyanometallate nanoparticles. Importantly, both novel nanosensitizers (Pt[Pt(CN)<sub>4</sub>] and Pt[Fe(CN)<sub>6</sub>]) are prepared in fairly large quantities using a water-based, surfactant-free, green route. The post-coating of the inorganic cores by different biocompatible polymers is straightforward and allows probing the influence of coating on the radiotherapeutic efficiency of the nanosystems. The structural/chemical integrity is maintained after high doses of  $\gamma$ -radiation and high colloidal stability is obtained in biological media. At 250  $\mu$ M total metal concentration, these nanoparticles are non-toxic to cells, but when coupled with  $\gamma$ -radiation, they amplify apoptosis of HeLa cells by 20% at 4.5 Gray, which rises up to 60 % at larger doses. Furthermore, irradiation studies conducted on a model DNA probe evidence that in the presence of these novel Pt-based radiosensitizers, the amount of lethal Double Stranded Breaks (DSB) is significantly enhanced. The radiotherapeutic efficiency of these versatile coordination nanoparticles obtained using a cheap, fast and green process opens interesting possibilities in the field of nanomedicine.

### Introduction

Even in the 21st century, cancer remains one of the biggest healthcare challenges with 19.3 million new cases detected in 2020, resulting in 10 million deaths all across the globe.<sup>(1)</sup> There is widespread ongoing research to develop targeted, safe and patient-specific treatment methods. Radiation therapy is applied to more than 50% of cancer patients to eliminate cancerous tissues in a localised way while minimizing the chances of recurrence in the affected area. A major advantage of radiotherapy is that tumours located deep within the body could also be targeted using the high energy X-rays,  $\gamma$ -rays or ion beams as their penetration depth is greater than 10 cm.<sup>(2)</sup> However, a high dose of these ionizing radiations can damage the healthy tissues and organs adjacent to the tumour, cause adverse side-effects like severe fatigue, radiodermatitis and in some cases, even second cancers due to mutations generated during the process.<sup>(3)</sup> Therefore, many radio-enhancers have been developed over the past two decades in order to maximize the cancer cell killing while working within a safe range of therapeutic dose of radiation. These agents need to be stable, non-toxic to normal tissues and fairly resistant to metabolic breakdown.<sup>(4)</sup>

It was recently documented that irradiating cells internalized with high-Z elements, generated a cascade of Auger electrons.<sup>(5)</sup> These secondary electrons are brought about by inner shell ionization of heavy metal atoms which lead to a significant increase in the amount of reactive oxygen species (ROS) produced upon water radiolysis. When these radicals are generated in close proximity to the cancer cells, their proliferation is stalled, causing apoptosis and subsequent elimination. In 2004, J.F. Hainfield et al provided the first proof of concept that gold nanoparticles (NPs) significantly improved the *in vivo* efficacy of radiation therapy. They demonstrated that the ultra-small size of these particles prove advantageous for bio-distribution and relatively high concentration of the heavy metal could be incorporated without toxicity.<sup>(6)</sup> The potential of metallic NPs in enhancing the local dose deposition of radiation was realised, and this led to an exponential increase in development of varied particles that could improve the performance of conventional radiation therapy. Additionally, nanoparticles provide a relatively large surface area and are flexible towards size, shape and charge modifications that prove advantageous for drug encapsulation and their delivery to target sites.<sup>(7)</sup> Few of the NPs developed for radiotherapy like gold (CYT-6091 Cytimmune)<sup>(8)</sup>, gadolinium-based (AGuiX, NHTheraguix)<sup>(9)</sup> and hafnium oxide-based nanoparticles (NBTXR3, Nanobiotix)<sup>(10)</sup> have even reached the clinical trial phase. Besides precious metal based radio-enhancers, rare-earth element based, semiconductor and even non-metallic NPs have been explored over the past few years. (11–15)

<sup>a</sup> Address here.

<sup>b</sup> Address here.

<sup>c</sup> Address here.

† Footnotes relating to the title and/or authors should appear here.

Electronic Supplementary Information (ESI) available: [details of any supplementary information available should be included here]. See DOI: 10.1039/x0xx00000x

However, most synthesis methods require multiple steps, use organic solvents, reducing agents and surfactants for controlling the nanoparticles' growth. Also subsequent functionalization and additional steps of purification is often required to make them water-soluble and biocompatible.(16) Such complications could be avoided by using a radiolytic method for synthesis and as Leza et al showed, monodisperse Pt NPs were prepared in a one-pot manner using  $\gamma$ -radiation. These particles efficiently enhance the effect of both proton and medical carbon beams on cancer cells.(17,18). But the scarce availability of a cobalt-60 radiation source to perform the synthesis of these nanoparticles, reduces its feasibility. So it is important to develop a green and simple synthetic procedure for generation of a new class of radio-enhancing agents.

It was recently demonstrated that the microporosity of a nanostructure could amplify the production of ROS and facilitate their diffusion after irradiation. Li et al showed for the first time that the porous structure of 200 nm MIL-100 iron (Fe) nanoMOFs not only serve as a cargo to release drug molecules but also participate as efficient radiation enhancers due to the presence of well-dispersed Fe centres. (19) Another family of microporous coordination nanoparticles related to Prussian Blue (PB) and polycyanometallate network for improving radiation therapy, has been envisaged in our study. PB is a famous pigment and the oldest microporous coordination polymer. It is a FDA-approved compound known as Radiogardase® and is used for radioisotope decontamination.(20) Since the last decade, many new and exciting biomedical applications of PB-based nanostructures have been discovered and their applicability in photothermal therapy (PTT), chemotherapeutic drug delivery and multimodal imaging (MRI, PET, PAI) has been demonstrated.(21) In 2020, Ren et al reported 200 nm, hollow mesoporous PB NPs doped with radio-sensitizing Bismuth nanodots for achieving combined photo-thermal and radiation therapy.(22) Besides PB, nanoparticles of related polycyanometallate coordination networks with different compositions have been studied for their magnetic and optical properties, applications in catalysis, batteries as well as electrochromic devices. (23,24)

Some/our? groups have reported the synthesis of such versatile coordination NPs using a fast and green surfactant-free, water-based method while maintaining a sub-10 nm size.(25–28) These nanoparticles gather many advantages: (i) a high proportion of metal atoms are located at the surface (50% for 4 nm nps) of the particle due to its porous nature (ii) easy combination of different metals in precise proportions is possible, either within the core or by a controlled growth of core-shells and (iii) a straightforward post-coating of NPs by polymers/molecules without changing the inorganic core could be obtained, enabling systematic comparisons. Unlike nanoMOFs, these nanoparticles are stable even in diluted conditions and do not dissolve. It was hypothesised that since such polycyanometallate based NPs are also intrinsically porous, irradiation in the presence of water could increase the production of reactive radicals. Application of such ultrasmall

PB-related compounds for radiation therapy is a widely unexplored field. Therefore, we aimed at creating a new family of radioenhancers made up of porous Pt-containing coordination networks.

Two novel Pt-based nanostructures ( $\text{Pt}[\text{Fe}(\text{CN})_6]$  and  $\text{Pt}[\text{Pt}(\text{CN})_4]$ ) are reported in this study. Hereafter, for the sake of simplicity they will be referred to as PtFe and PtPt NPs. The effect of radiation beams on HeLa cells in the presence of these self-standing, coordination nanosystems is examined. The use of DNA plasmid as a model system to understand the molecular scale mechanisms occurring in the presence of our NPs and radiation is also discussed.

## Results and Discussion

### Synthesis and characterization of Pt-based nps

The synthesis of two new transition metal co-ordinated, self-standing nanoparticles containing high-Z metals has been described in section . The one-step reaction was carried out in pure water, under easily reproducible conditions. A Pt(II) salt was used in the experimental procedure in order to incorporate a high-Z metal in the NP. Once the activation temperature was reached, addition of  $\text{K}_2\text{PtCl}_4$  to the corresponding metal (Pt/Fe) cyanide solution, triggered the gradual substitution of chloro (-Cl) ligands by the cyano (-CN) ligands. This could be followed by a certain change in colour of the reaction mixture depending on the precursors used. The reaction time, temperature, ratio of precursors, and amount of polyvinylpyrrolidone (PVP) polymer added play a crucial role in the final structure and composition of the NPs.

TEM micrographs reveal homogenous and spherical PtFe and PtPt nanoparticles. The size distribution histograms (Figure 1) calculated by averaging the sizes of 200 nps, reveal that PtFe particles have a core average diameter of  $5.2 \pm 1.0$  nm and PtPt are much smaller at  $1.2 \pm 0.4$  nm. Due to intense absorption of the green coloured PtFe colloidal solution in the laser absorption region, the hydrodynamic diameter obtained was not very reliable. DLS measurements indicated that the hydrodynamic diameter of synthesized PtPt NPs was  $9.9 \pm 3.9$  nm which appeared to increase by  $\sim 3$  nm in three days. However, addition of PVP after the synthesis arrests the growth and the sub-10 nm size is maintained (Supplementary Fig). The zeta potential of PVP coated PtFe and PtPt in water were around  $-23.5 \pm 5.3$  mV and  $-26.7 \pm 5.9$  mV respectively. The presence of polycyanometallate complex at the surface of the NPs explains the negative charge and their long-term stability in the colloidal solution. The strong electrostatic repulsions prevent aggregation of the particles and helps maintain their size and shape in polar solvents as well as biologically relevant media like PBS and NaCl.

### Spectroscopic Analysis

Infra-red (IR) spectroscopy is a powerful characterization technique for these nanoparticles. The sensitivity of the cyanide stretch ( $\nu(\text{CN})$ ), depends highly on its chemical environment,

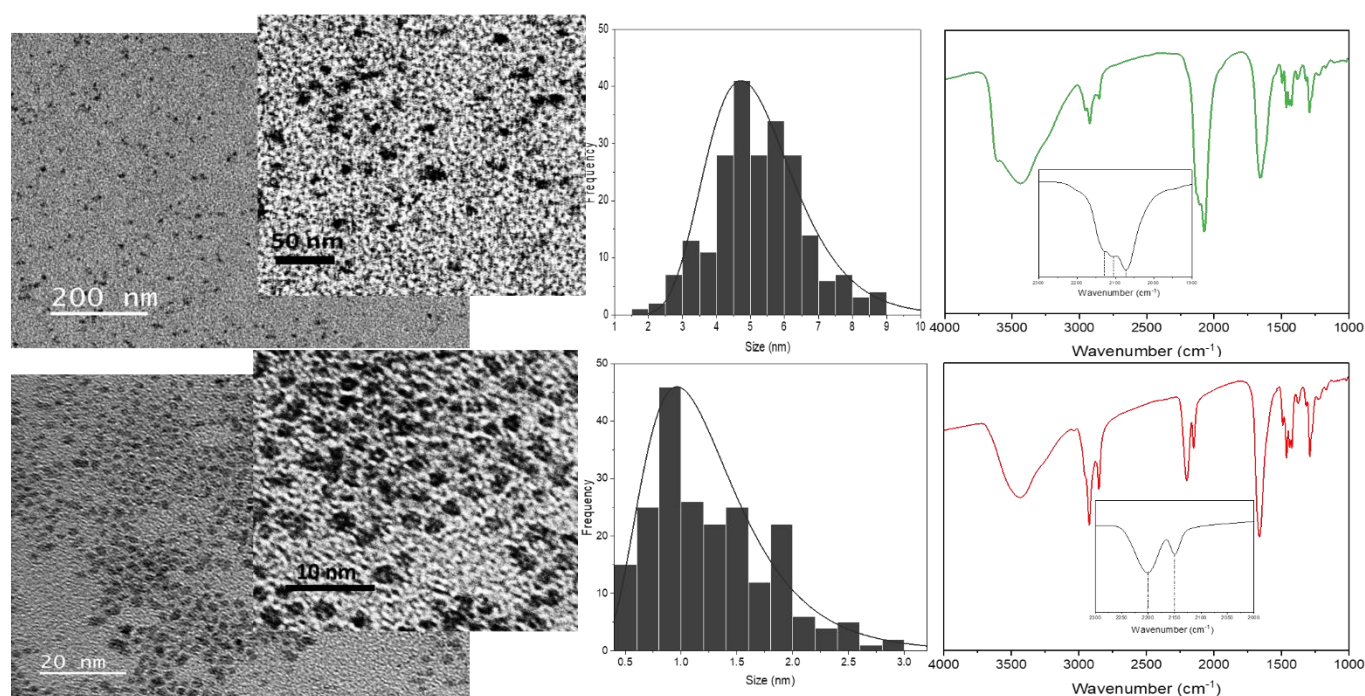


Figure 1. TEM micrographs of PtFe NPs (top) and PtPt NPs (bottom) at different magnifications, with their corresponding size distribution charts and infra-red spectra.

especially the linked metal centre (M-CN) and this was used to ascertain changes occurring during the synthesis. In the PtFe NP spectra, the peak at  $2109\text{ cm}^{-1}$  could be attributed to the vibrations of the bridging cyanide between the two metals ( $\text{Fe}^{\text{II}}\text{-CN-Pt}^{\text{II}}$ ), while the shoulder at  $2130\text{ cm}^{-1}$  corresponds to terminal  $\text{Fe}^{\text{III}}\text{-CN}$ . A peak is also observed at  $2072\text{ cm}^{-1}$  which is a characteristic of PB ( $\text{Fe}^{\text{II}}\text{-CN-Fe}^{\text{III}}$ ) pairs. UV-Visible spectroscopy also confirms the formation of  $\text{Fe}^{\text{III}}$  during the synthesis (supp.figure). The intense absorption peak in the  $300\text{-}400\text{ nm}$  region corresponds to charge transfer within  $\text{Fe}^{\text{II}}\text{-CN-Pt}^{\text{II}}$  pairs forming the coordination network, while the broad band around  $750\text{-}820\text{ nm}$  indicates the presence of PB pairs. Comparing their molar absorption coefficients with PB, it could be deduced that the number of such  $\text{Fe}^{\text{II}}\text{-CN-Fe}^{\text{III}}$  pairs formed are extremely small, amounting to roughly 3.5%. So the oxidation of  $\text{Fe}^{\text{II}}$  to  $\text{Fe}^{\text{III}}$  during the synthesis is very minimal. The IR analysis of PtPt NPs show a clear shift of about  $25\text{ cm}^{-1}$  with respect its tetracyanoplatinate(II) precursor. The peak at  $2150\text{ cm}^{-1}$  corresponds to terminal  $\text{Pt}^{\text{II}}\text{-CN}$  stretch and the intense vibration of bridging cyanide ( $\text{Pt}^{\text{II}}\text{-CN-Pt}^{\text{II}}$ ) is detected at  $2201\text{ cm}^{-1}$ . The characteristic vibrations of C=O stretch at  $1660\text{ cm}^{-1}$ , ternary CN at  $2854\text{ cm}^{-1}$  and symmetric  $\text{CH}_2$  stretch at  $2920\text{ cm}^{-1}$  from PVP was an indication of polymer coating.

The formula unit of these novel nanosystems were determined using energy dispersive spectroscopy to be  $\text{K}_{1.2}\text{Cl}_{0.4}\text{Pt}[\text{Fe}(\text{CN})_6]_{0.7}$  for PtFe and  $\text{K}_{0.1}\text{Cl}_{0.1}\text{Pt}[\text{Pt}(\text{CN})_4]$  for PtPt NPs. XPS analysis of the deposited PtFe powder provides clear indication of presence of iron in  $\text{Fe}^{\text{II}}$  state with its 2p edge located at  $708.3\text{ eV}$ . The Pt binding energy (BE) has shifted to slightly lower values compared to tetracyanoplatinate precursor ( $73.9$  to  $73.5\text{ eV}$ ) which could be attributed to  $\text{Pt}^{\text{II}}$  linked through the N end of the cyanide bridge. The analysis of PtPt powder shows that

platinum metal retains its +II oxidation state in the NP with binding energy peaks centered at  $73.8$  and  $77.1\text{ eV}$ . The deconvolution of N 1s and C 1s core level peaks obtained in the survey could be assigned to the CN bond between the metals as well as the C-N and C=O bonds coming from the PVP polymer coating. The geometries of constituent complexes and the spectroscopic results suggest that the structure of  $\text{Pt}[\text{Fe}(\text{CN})_6]$  is similar to that of a PB analogue but with a many vacancies and defects due to incomplete replacement of Cl with CN in the NP.  $\text{Pt}[\text{Pt}(\text{CN})_4]$  is made of sheets of  $[\text{Pt}(\text{CN})_4]$  surrounded by 4 Pt(II) atoms. Due to their ultras small size and presence of defects, X-Ray powder diffraction did not reveal any clear peaks.

#### Evaluation of stability in physiological media and irradiation

It was observed that the NP solutions were stable at room temperature and could be stored over long periods of time without change in composition at  $4^\circ\text{C}$ . The consequence of exposure to biological medium was analysed by dispersing the nanoparticles in Foetal Bovine Serum (FBS). The evolution was studied using UV-Visible spectroscopy at the normal body temperature of  $37^\circ\text{C}$ . PtFe NPs underwent very minimal change over the course of 15 hours in FBS. The minor peaks at  $414\text{ nm}$  and  $772\text{ nm}$  which correspond to a small amount of  $\text{Fe}^{\text{III}}$  present in the NP, experience a slight decline over time. This is due to the high affinity of phosphate present in the serum, towards ferric ions. However, the major band representing  $\text{Fe}^{\text{II}}\text{-CN-Pt}^{\text{II}}$  that is integral for the nanoparticle structure undergoes no degradation. Similarly the  $\text{Pt}^{\text{II}}\text{-CN-Pt}^{\text{II}}$  band around  $306\text{ nm}$ , in PtPt NPs remains unaffected over 15 hrs at  $37^\circ\text{C}$ . These studies provide an indication that these polycyanometallate based coordination NPs would remain stable during its transport within the human body.

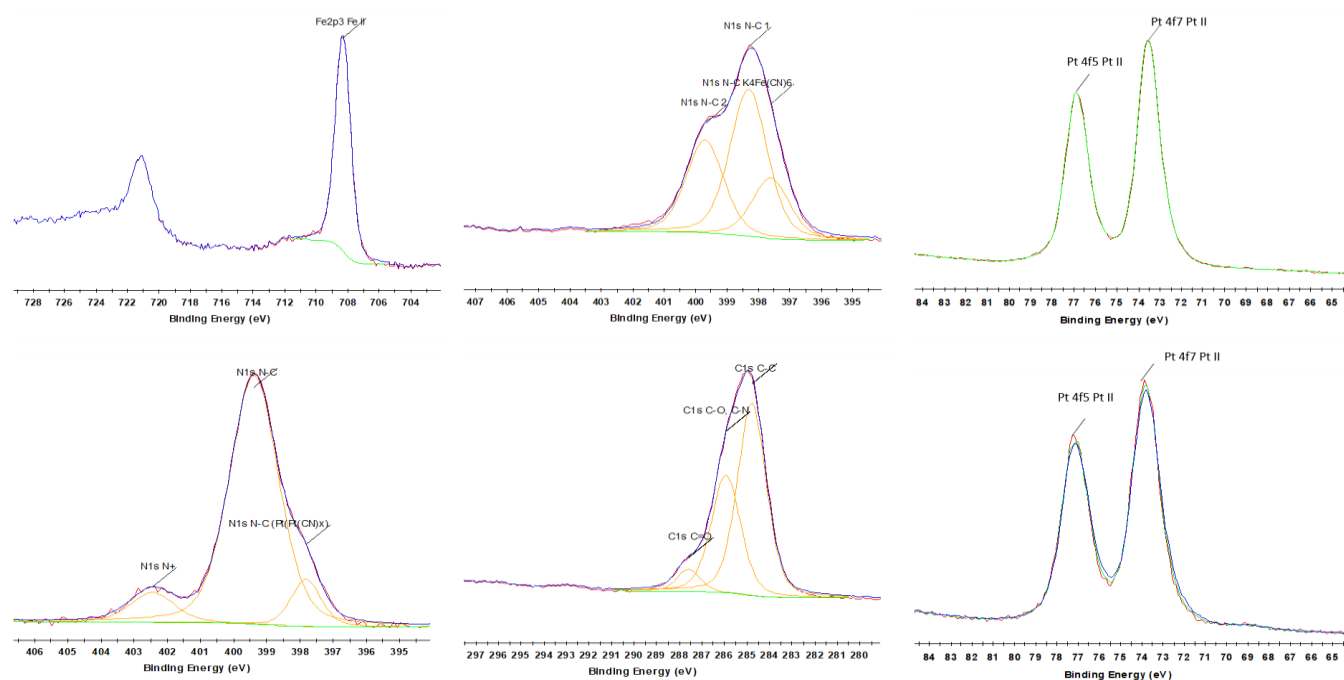


Figure 2. XPS spectra of PVP coated PtFe NPs (top) in regions (a) Pt-4f (b) N-1s (c) Fe-2p and PtPt NPs (bottom) in (d) Pt-4f (e) C-1s (f) N-1s core levels.

Similar tests were run in Artificial Lysosomal Fluid (ALF) and the evolution of the absorption spectra was studied for a duration of 6 hours. The major peaks of both NPs underwent no change even in this acidic medium. A small increase in intensity could be seen in the peaks corresponding to  $\text{Fe}^{\text{III}}$  which is attributed to slight oxidation of  $\text{Fe}^{\text{II}}$  under such conditions. Altogether, it could be concluded that these novel nanoparticles are not damaged by the cellular medium and could be used for further tests.

In order to evaluate the viability of the NPs as radio-enhancing agents, their stability in presence of radiation was investigated. Both the NP solutions, as well as their control samples (precursors) in the presence of PVP and dextran polymers were subjected to a gamma-radiation dose of 4 kGy. Upon irradiation, reactive oxygen species (ROS) are generated in solution. The ROS play a crucial role in enhancing the effect of radiation on the targeted cancer cells. They are capable of oxidising  $\text{Fe}^{\text{II}}$  to  $\text{Fe}^{\text{III}}$  and this is substantiated by the appearance of a new band around 425 nm after irradiation of ferrocyanide control solution. However, in the presence of dextran polymer, this ferricyanide band was not formed indicating no oxidation had taken place. This indicated that dextran is capable of scavenging the ROS formed and therefore is not an ideal material for coating nanoparticles developed for radiation therapy. Since PtFe and PtPt nanoparticles could easily be post-coated, the synthesis was optimised to include PVP polymer. Presence of PVP does not hinder ROS generation as evidenced by the LMCT band in the irradiated ferrocyanide + PVP sample (Suppl. Fig). DLS, TEM and UV-Visible spectral analysis performed before and after radiation showed that PtFe and PtPt nanostructures are not significantly altered. Hence, they would remain stable during the course of radiation treatment.

#### Cytotoxicity, uptake and radiation effects of nanoparticles in cells

The primary fibroblasts are biologically relevant tools for measuring toxicity of nanoparticles towards healthy cells, while HeLa can provide an indication of their behaviour towards cancerous cells. The effect of a range of [M] in PtFe and PtPt nps were tested in both cell lines incubation time of 6 h (Figure 5). The columns represent average survival fractions with respective deviation values. According to the international standard for biological evaluation of medical devices, a sample is considered non-cytotoxic when even the highest concentration provides 70% cell-survival.<sup>(29)</sup> The fibroblast cell viability is close to 80% at the highest metal concentration ([M]) of  $1 \times 10^{-3}$  M for both nanoparticles indicating their safety for medical applications. HeLa cells appear more sensitive to the presence of nanoparticles as they reach the same limit at  $5.0 \times 10^{-4}$  M concentration. The [M] of  $2.5 \times 10^{-4}$  mol.L<sup>-1</sup> was considered safe for these cells and hence this concentration was maintained for further experiments.

ICP-OES analysis of HeLa (ca.  $1.3 \times 10^6$ ) cells incubated with PtFe NPs for 6 h showed that a total of 73 ng of Pt was internalized. Therefore, 0.28 fmol of this high-Z element was taken up by one cell. In the case of PtPt NPs, 182 ng of platinum was detected in ca.  $1.8 \times 10^6$  HeLa cells, meaning the amount of Pt internalized was approximately 0.52 fmol/cell. The impact of these particles in cell killing was studied using  $\gamma$ -rays from a Cesium-137 source (0.63 MeV). The cancer cells incubated with NPs were irradiated for different time intervals at a dose rate of 0.75 Gy/min. The colonies formed at the end of standard 14 day incubation period helped determine the survival fraction (SF) at each dose. The colony count data was fit using a linear-quadratic model (LQM) on a logarithmic scale (SF vs dose) using equation 1:

$$SF(D) = e^{-(\alpha D + \beta D^2)} \quad (1)$$

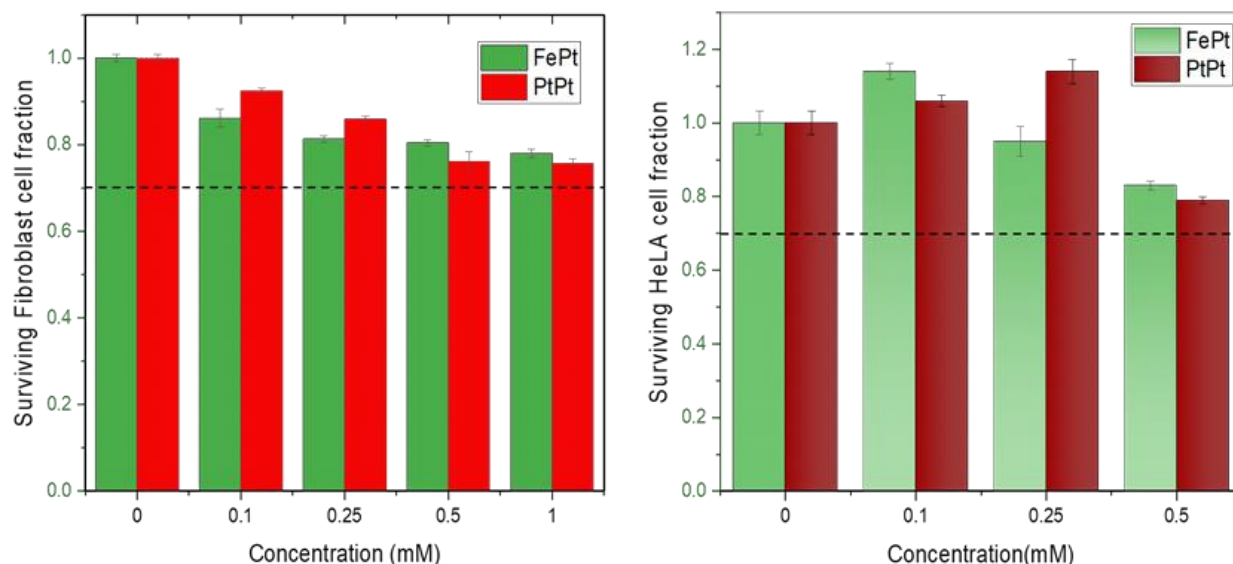


Figure 3. The *in vitro* toxicity results of PtFe and PtPt NPs evaluated by clonogenic assay using (a) Fibroblast cells and (b) HeLa cells after 6 h incubation. Dotted line represents the safety limit according to ISO 10993-5.

here  $D$  corresponds to dose supplied, while parameters  $\alpha$  and  $\beta$  describe the cell's radiosensitivity.  $\alpha$  represents the induction of directly lethal damages whereas  $\beta$  term corresponds to additive sub-lethal lesions leading to cell death. The  $\alpha/\beta$  provides the dose (Gy) at which 50% of the damages caused to the cells are due to directly lethal effect of radiation while the rest are a result of additive damages triggering a lethal consequence.

The percentage of surviving cells sequentially decreased as a result of radiation but as presented in Figure 6, this decline is significantly amplified in the presence of PtFe and PtPt NPs. This proves the radioenhancing nature of these novel polycyanometallate based NPs. The effectiveness of NPs as

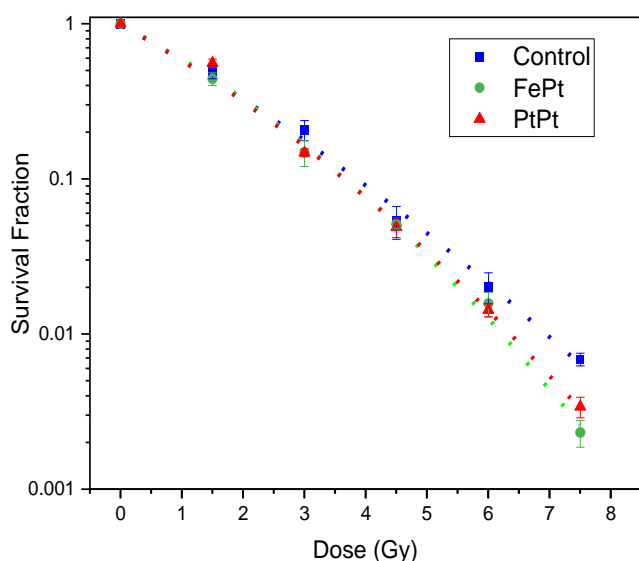


Figure 4. Survival fraction of HeLa cells after radiation with Cs-137 without NPs (blue), in presence of 0.25 mM PtFe (green) and PtPt (red) nanoparticles, fit using LQM (dotted lines) as a function of dose.

radioenhancers could be quantified by means of Dose Enhancement Factor (DEF). It gives the measure of efficiency of *in vitro* cell killing at a given dose point ( $D$ ) and was calculated using the following equation:

$$DEF = SF_{control,fit} / SF_{NP,fit} \quad (2)$$

here,  $SF_{control}$  and  $SF_{cyanosol}$  correspond to the survival fractions of cells incubated without and with PtFe/PtPt nps at the same dose of radiation from the fitted curve. Until a radiation dose of 4.5 Gy, both the NPs behave similarly and a DEF of  $\sim 1.25$  is obtained. As the dose supplied to the sample increases, high DEF values upto 1.92 for PtPt and 2.45 for PtFe could be observed. This corresponds to a 48% and 59% raise in the cancer cell killing rate in the presence of  $2.5 \times 10^{-4}$  mol.L<sup>-1</sup> PtFe and PtPt NPs. As reported in Table 1, the alpha values in all three cases are quite similar, indicating that the number of directly lethal damages produced as an effect of radiation does not change much in the presence of these NPs. However, the  $\beta$  value shifts from  $2.1 \times 10^{-2}$  Gy<sup>-2</sup> in the control experiment to  $3.4 \times 10^{-2}$  Gy<sup>-2</sup> for PtPt. In case of PtFe NPs, the  $\beta$  is more than double that of the control, at  $4.4 \times 10^{-2}$  Gy<sup>-2</sup>. This significant increase of  $\beta$  value indicate that the radioenhancing mechanism of such polycyanometallate NPs are quite unique as they first produce a high amount of sub-lethal damages, which then add up and lead to cancer cell death.

Table 1. Values of  $\alpha$  and  $\beta$  obtained from the fitting curve for NPs and control experiment in HeLa cells in the presence of radiation.

Sample	$\alpha$ (Gy <sup>-1</sup> )	$\beta$ (Gy <sup>-2</sup> )	$\alpha/\beta$ (Gy)
Control	$0.515 \pm 0.050$	$0.021 \pm 0.007$	$24.30 \pm 9.44$
PtFe	$0.464 \pm 0.050$	$0.044 \pm 0.008$	$10.57 \pm 2.21$
PtPt	$0.500 \pm 0.049$	$0.034 \pm 0.007$	$14.38 \pm 3.56$

Here, it can be hypothesized that water molecules coordinated to the surface of the NP as well the ones constantly diffusing through porous network are available for conversion to ROS. Compared to the control, the presence of Pt increases the number of radicals formed in solution due to the Auger effect. It is possible that due to the microporosity of the NP, ROS generated is quickly dispersed through the biological system causing markedly high amount of sub-lethal damages that is transformed to a final lethal effect in the cell. It has to be noted that despite the presence of a lower amount of high-Z element in PtFe NP, they produce similar and sometimes even better amplification of radiation damage, when compared to PtPt NPs. This could be due to two reasons. The  $\gamma$ -radiation interacts with Fe atoms as well and following a combination of various phenomena (activation, de-excitation and emission of electrons) also lead to the production of toxic radicals that help with cell killing.<sup>(19)</sup> Secondly, as compared to the 2D sheets that form PtPt NP, the PtFe nanostructure is a Prussian Blue-like structure full of defects and vacancies, that can be occupied by water molecules. This could mean that more reactive radicals are formed within and around PtFe NP and they have higher freedom of mobility and undergo faster diffusion throughout the cell media. This is further proof that microporosity of the nanostructure used in radiation therapy heavily affects the final results. It can be concluded from the data that even at low concentrations, both the nanoparticles cause death of targeted cells and positively improve the lethality of  $\gamma$ -radiation.

#### Radio-induction of nanoscale damage

It has been hypothesised that high-energy radiation beams induce irreparable damages on cell organelles, proteins and nucleic acids by producing ROS, during water radiolysis. These nanometric damages on biomolecules lead to mutations, cell death and subsequent elimination, and is the working principle behind radiotherapy for cancer. In order to study the impact of cyanosols to bring about these complex damages, plasmids were used as bio-nanoprobes. They were incubated with PtFe and PtPt NPs ( $[M]=5.3 \times 10^{-6} \text{ mol.L}^{-1}$ ) subjected to varying dose of radiation. The intact form of the plasmid exists in a supercoiled conformation. Break in these circular double-stranded model-DNA diminishes the constraints in the structure and leads to formation of relaxed (R') and linear conformations (L'). The three forms of DNA could be separated by gel electrophoresis and the detected amount of each enables quantification of single and double strand breaks. As described in the experimental section, the amount of DSBs were calculated using amount of L' that rose out of irradiating plasmid pBR322.

The number of lethal, nanometric DSBs generated are presented as a function of radiation dose (0 - 160 Gy) in Figure 7. As expected, the number of nanosized breaks rises with an increase in the dose of radiation applied to the samples. But in the presence of PtFe and PtPt NPs, the amount of damages are significantly enlarged and was quantified using sensitizer enhancing ratio (SER).

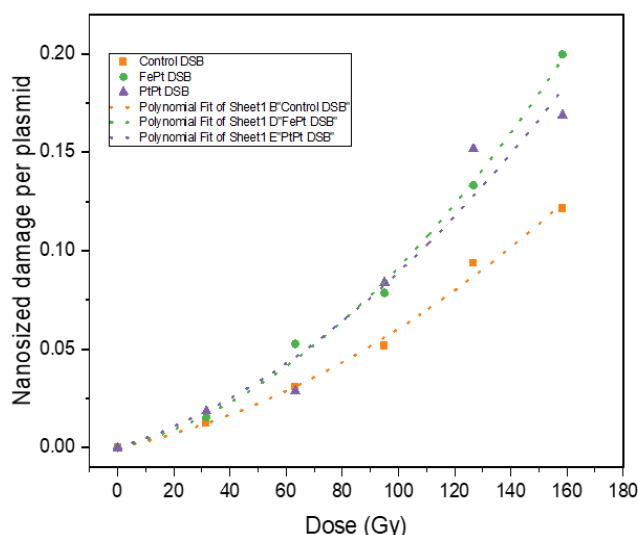


Figure 5. Nanometric damages induced by  $\gamma$ -radiation in plasmid nanoprobes without NPs (orange) and in presence of PtFe (green), PtPt (purple) NPs and their respective fitted curves.

$$SER = DSB_{NP} / DSB_{control} \quad (6)$$

here,  $DSB_{control}$  corresponds to the number of nanoscale damages per plasmid upon a certain dose of radiation while  $DSB_{NP}$  indicates the same in presence of plasmid loaded with NP solution.

It is interesting to see that with PtPt, irrespective of the dose supplied, an almost constant enhancement in double strand breaks in the range of 46–49% is obtained. On the other hand, FePt nanoparticles produce a comparatively smaller effect at low doses (SER 1.34 at 30 Gy) and sequentially intensifies its damage to the DNA with increasing dose of radiation (1.59 at 160 Gy). The aim of radio-enhancers is to maximize the amount of damages to the cancerous cells, instigate quick apoptosis and minimize the possibility of regeneration while applying a therapeutic dose of radiation. Therefore, even the lowest amplification in DSBs (here 30%) in the presence of these porous coordination nanoparticles, synthesized in a green and inexpensive manner is very significant. Here, we have demonstrated that at a minimal concentration of  $5.3 \times 10^{-6} \text{ mol.L}^{-1}$ , both nanoparticles amplified the effect of radiation, indicating clearly that they act as radiation-enhancing agents. These experiments help in understanding the molecular mechanisms behind radiation treatment.

The results further prove that the complex damages occurring to the biomolecules is the root cause of amplification in cell death observed with the clonogenic assay. Similar to the results obtained with experiments conducted on cells, the bi-metallic PtFe NPs appear to be more effective in causing these damages than pure Pt coordination nanostructures at high doses.

#### Conclusions

The present study reported a green, cheap and fast synthetic procedure of two novel Pt-containing polycyanometallate

based nanostructures. Complete characterization revealed that these ultra-small, negatively charged, bi-metallic coordination nanoparticles are well-individualised and stable in water as well as physiological media like FBS and ALF. These PtFe and PtPt nps could be easily post coated with polymers depending on the targeted applications and they remained intact upon irradiation which suggested their applicability as radioenhancers. A marked increase in lethal double strand breaks on model DNA were observed in the presence of these newly-synthesised NPs. The *in vitro* tests revealed that they were non-toxic to primary fibroblast and HeLa cells in a good range of concentrations. However, irradiation of the cells containing the NPs with an ionizing beam induced a strong cytotoxicity, with the amplification factor rising up to 59%. Therefore, our cyanide bridged PtFe and PtPt NPs could serve as an effective agent that amplify the damages on cancer cells at therapeutic doses. Interestingly, the PtFe reveal improved effect that could be related to the 3D Prussian Blue-like structure which is more porous than its PtPt counterpart. Moreover, as demonstrated by our group on some PB-like NPs, post-modification of the inorganic core could be easily done using coordination chemistry. Doping with paramagnetic ions (Mn(II), Gd(III) and Fe(III)) could impart strong MRI contrast properties to these NPs and lead to new and efficient theranostic nanoplatforms for image-guided treatments.

## Experimental Section

### Materials

Potassium ferrocyanide ( $K_4Fe(CN)_6$ ), Potassium tetrachloroplatinate ( $K_2PtCl_4$ ), Potassium tetracyanoplatinate ( $K_2Pt(CN)_4 \cdot 3H_2O$ ), Polyvinylpyrrolidone ( $C_6H_9NO$ ) (PVP MW 3500), dextran and hexadecyltrimethylammonium bromide (CTAB) were purchased from . Agarose D5 (Type D-5-DNA Grade from EUROMEDEX), Tris-Acetate-EDTA (TAE, 50x), Tris EDTA (TE) (1x), DNA (pBR322, 0.5  $\mu g/\mu L$ , from molecular biology), 6xDNA loading dye (#R0611, molecular from biology), Ethidium Bromide (EB, ref: EU0070, 10 mg/mL, molecular biology Grade, from EUROMEDEX). Distilled water was used for all the experimental procedures.

### Preparation of nanoparticles

This paper reports the preparation of two polycyanometallate based nanoparticles. The conditions for the most optimized sample are reported. For obtaining PtFe NPs,  $K_4Fe(CN)_6 \cdot 3H_2O$  (10mM) and  $K_2PtCl_4$  (10mM) solutions were prepared in distilled water and heated to reach the temperature of 55°C.  $K_2PtCl_4$  solution was added in one go into the  $K_4Fe(CN)_6 \cdot 3H_2O$  solution under vigorous stirring. The mixture turned yellow in colour and the reaction was run for 1 h while maintaining the temperature. The solution was cooled down to room temperature and turned dark green in colour.

In case of PtPt NPs, the precursor solutions  $K_2Pt(CN)_4 \cdot 3H_2O$  (10mM) and  $K_2PtCl_4$  (10mM) were prepared in water, and heated until the activation temperature of 85°C was reached.  $K_2PtCl_4$  was quickly added to the metal cyanide solution under

constant stirring. Initial colour of the solution mixture is brown, but as the reaction progresses (1h, 85°C) it becomes a colourless solution. The reaction was stopped and solution was brought to room temperature.

### Polymer coating

PVP monomer solution (150 mM) was prepared in water and added to preformed NP solution under constant stirring. After 30 minutes, the solution was ultra-filtered and washed twice with distilled water to remove excess reactants. This solution was utilised for characterization and biological tests.

About dextran coating too? Lucile data?

CTAB (5mM) in methanol was added to a part of cyanosol solutions to induce flocculation. The mixture was centrifuged at 2°C until a pellet was formed. It was dried under vacuum for several hours and the powder obtained was used for further characterization.

### Physicochemical characterization

The hydrodynamic diameter and zeta potential of each prepared sample were determined using Zetasizer NanoZS (Malvern instruments, UK) equipped with backscattering mode. Multiple batches of the sample were analyzed with standard disposable polystyrene and DTS 1070 cuvettes, and the mean values are reported with corresponding standard deviation. Transmission electron microscope (TEM JEOL 1400, Japan) operating at an accelerating voltage of 120 kV, was used to observe the size and dispersity of the sample. Formvar coated copper grids were glow-discharged before placing a few drops of PtFe and PtPt NP solution. The characteristic chemical bonds making up the structure of the nanoparticles were verified using FT-IR spectrophotometer (Perkin Elmer Spectrum 100) using KBr pellets. Energy dispersive spectroscopy (EDS) and X-ray photoelectron spectroscopy (ThermoFisher Scientific K-Alpha) measurements were performed to understand the elemental composition and determine the oxidation state of metals in the final sample.

### Irradiation studies

Cobalt-60 gamma source (1.25 MeV) at Institute of Physical Chemistry (ICP), University Paris Saclay was used as the radiation source for the experiments. PtFe and PtPt cyanosols synthesised with PVP and dextran coating along with their precursors:  $K_4Fe(CN)_6$ ,  $K_4Fe(CN)_6$ +PVP,  $K_4Fe(CN)_6$ +dextran,  $K_2Pt(CN)_4 \cdot 3H_2O$  and  $K_2Pt(CN)_4 \cdot 3H_2O$ +PVP were analysed before and after irradiation to evaluate changes occurring in presence of high energy beams. Each sample was degassed with  $N_2O$  and irradiated for an hour at a dose rate of 4kGy/hr.

### Radio-sensitizing effect on DNA: sample preparation and analysis

The plasmid pBR322 (Fisher Scientific in 10mM Tris-HCl, 1mM EDTA) was used as a bio-nanoprobe to understand the radio enhancing effect of prepared nanoparticles. It consists of circular double stranded DNA of 4361 base pairs ( $2.83 \times 10^6$  Da) with 95% in native supercoiled (S) conformation and approximately 5% in the relaxed (R) conformation. It arises as a

result of single strand breaks (SSB) in DNA while double strand breaks (DSB) are caused by two breaks in two strands separated by less than 10 base pairs. DSB leads to linear (L) conformation in the plasmid and this form is absent in the native product.

Each sample was prepared by using 10  $\mu\text{g}$  of DNA (10  $\mu\text{L}$ ) in 123  $\mu\text{L}$  Tris-EDTA buffer solution. The plasmid was incubated with each nanoparticle solution (24  $\mu\text{L}$ ) for one hour to ensure binding. The stock solution was diluted to attain total metal (Fe/Pt+Pt) concentration of  $5.3 \times 10^{-6}$   $\text{mol.L}^{-1}$  and final volume was adjusted to 180  $\mu\text{L}$  using milli-Q water (18.2  $\text{M}\Omega\cdot\text{cm}$  at 25°C). A control sample was prepared simultaneously containing plasmid with 24  $\mu\text{L}$  of water to present the effect of radiation in the absence of radio-enhancers. Each sample was split into 6 aliquots (18  $\mu\text{L}$  each) and exposed to  $\gamma$ -radiation with the applied dose ranging between 0 – 158 Gy.

The damaging effect of irradiation was quantified by analysis of linear, relaxed and supercoiled conformation in the sample using agarose gel electrophoresis. 14-well (1% agarose) gels were prepared in Tris-Acetate-EDTA (TAE) buffer and 9  $\mu\text{L}$  of each irradiated plasmid solutions were loaded in the wells together with a blue dye. The three forms migrated different distances by electrophoresis (80 V, 3 hr, 4°C), due to the difference in volume. The gel was stained using ethidium bromide (EB) solution, washed twice, studied under UV transilluminator ( $\lambda=302$  nm) and recorded by a CCD camera. The images were examined to calculate amounts of L, S and R conformations present in each irradiated sample. Since S binds 1.47 times less to EB than R and L, normalization was done and respective fractions of R (R'), S (S') and L(L') were calculated.

$$\text{Total} = 1.47 \times S + R + L$$

$$R' = R / \text{Total}$$

$$S' = 1.47 \times S / \text{Total}$$

$$L' = L / \text{Total}$$

The yield of nanosized damages (SSB and DSB) per plasmid were determined using the established formulae based on Poisson law statistics.<sup>18</sup>

$$\text{DSB per plasmid} = L' / (1-L') \quad (4)$$

### Cell viability studies

HeLa and primary dermal fibroblast cells purchased commercially from the American Type Culture Collection (CCL-2TM, LGC Standards S.a.r.l. - France Office), were cultivated in Dulbecco's Modified Eagle Medium (DMEM) (Life Technologies) enriched with 4.5 g/L glucose and supplemented with 10% heat-inactivated Fetal Bovine Serum (FBS), 1% antibiotics (100 U/mL penicillin and 100  $\mu\text{g}/\text{mL}$  streptomycin) and 1% Non-essential amino acids (all supplements from PAA Laboratories) and cultured at 37°C in 5% CO<sub>2</sub> atmosphere.

The toxicity of PtFe and PtPt nanoparticles were evaluated in both systems: healthy primary Fibroblast cells and cervical cancer-derived HeLa cells, using a colony formation assay. The cells were incubated with nanoparticle solutions containing total metal concentrations in the range of  $0.1-1.0 \times 10^{-3}$   $\text{mol.L}^{-1}$  for 6 hours. The colonies formed were fixed and stained using 0.5% methylene blue 50% (v/v) methanol solution and counted

manually. The control sample containing cells incubated with same amount of water was used to determine toxicity of nanoparticles at each concentration. Each data point was triplicated to incorporate a margin of experimental error.

### Uptake quantification

HeLa cells ( $2 \times 10^5$ ) were incubated with PtFe and PtPt nanoparticles for 6 h at a total metal concentration of  $2.5 \times 10^{-4}$   $\text{mol.L}^{-1}$ . At the end of incubation period, the culture medium was removed, the cells were rinsed with PBS solution and harvested after trypsinization. The cells were then counted using LUNA counter and centrifuged for 7 min at  $200 \times g$ . The supernatant was removed and the cell pellets were stored in glass tubes. Before analysis, the pellets were dissolved in aqua regia and diluted using ultrapure water. The quantification of platinum internalized within the cells, was performed at UT2A (Pau, France) by Inductively Coupled Plasma (ICP) analysis.

### Radio-sensitizing effect on cells

The impact of radiation on cell survival in the presence of prepared NPs was evaluated using a colony formation assay. HeLa cells were cultured in T25 flasks and maintained at 37°C overnight, in a humidified 95% air-5% CO<sub>2</sub> atmosphere. They were then incubated for 6 hours with enriched culture medium containing PtFe and PtPt nps at  $2.5 \times 10^{-4}$   $\text{mol.L}^{-1}$  total metal concentration. The cells with the nanoparticles, as well as the control containing an equivalent amount of water were irradiated using the Cs-137 (0.63 MeV) source at Institute Curie. The dose supplied ranges from 0 - 7.5 Gy. After the exposure, the cells were seeded onto petri-dishes to start the standard 14 days culture time. Colonies formed were fixed, stained and counted to determine survival fractions at each dose and the data obtained was normalized against the corresponding control. Each measurement was performed in triplicate and the average was used to calculate dose enhancement and amplification factors in presence of high-Z nanoparticles.

### Author Contributions

We strongly encourage authors to include author contributions and recommend using [CRediT](#) for standardised contribution descriptions. Please refer to our general [author guidelines](#) for more information about authorship.

### Conflicts of interest

In accordance with our policy on [Conflicts of interest](#) please ensure that a conflicts of interest statement is included in your manuscript here. Please note that this statement is required for all submitted manuscripts. If no conflicts exist, please state that "There are no conflicts to declare".

### Acknowledgements

The acknowledgements come at the end of an article after the conclusions and before the notes and references.

## Notes and references

‡ Footnotes relating to the main text should appear here. These might include comments relevant not central to the matter under discussion, limited experimental and spectral data, and crystallographic data.

- §  
§§  
etc.
- Sung H, Ferlay J, Siegel RL, Laversanne M, Soerjomataram I, Jemal A, et al. Global Cancer Statistics 2020: GLOBOCAN Estimates of Incidence and Mortality Worldwide for 36 Cancers in 185 Countries. *CA Cancer J Clin* [Internet]. 2021 May 1 [cited 2022 Jan 6];71(3):209–49. Available from: <https://onlinelibrary.wiley.com/doi/full/10.3322/caac.21660>
  - Chalmers M. How particle physics can be therapeutic. *Physics World*. 2003;16(8):32–3.
  - Dracham CB, Shankar A, Madan R. Radiation induced secondary malignancies: a review article. *Radiat Oncol J* [Internet]. 2018 Jun 1 [cited 2022 Jan 12];36(2):85. Available from: </pmc/articles/PMC6074073/>
  - Adams GE. Chemical radiosensitization of hypoxic cells. *Br Med Bull* [Internet]. 1973 Jan 1 [cited 2022 Mar 10];29(1):48–53. Available from: <https://academic-oup-com.ezproxy.universite-paris-saclay.fr/bmb/article/29/1/48/284686>
  - Kobayashi K, Usami N, Porcel E, Lacombe S, le Sech C. Enhancement of radiation effect by heavy elements. *Mutation Research/Reviews in Mutation Research*. 2010 Apr 1;704(1–3):123–31.
  - Hainfeld JF, Slatkin DN, Smilowitz HM. The use of gold nanoparticles to enhance radiotherapy in mice. *PHYSICS IN MEDICINE AND BIOLOGY Phys Med Biol*. 2004;49:309–15.
  - Wilczewska AZ, Niemirowicz K, Markiewicz KH. Nanoparticles as drug delivery systems. *Pharmacological Reports*. 2012;64(1734–1140):1020–37.
  - Libutti SK, Paciotti GF, Byrnes AA, Alexander HR, Gannon WE, Walker M, et al. Cancer Therapy: Clinical Phase I and Pharmacokinetic Studies of CYT-6091, a Novel PEGylated Colloidal Gold-rhTNF Nanomedicine. Available from: <http://aacrjournals.org/clincancerres/article-pdf/16/24/6139/1993761/6139.pdf>
  - Verry C, Dufort S, Villa J, Gavard M, Iriart C, Grand S, et al. Theranostic AGuIX nanoparticles as radiosensitizer: A phase I, dose-escalation study in patients with multiple brain metastases (NANO-RAD trial). *Radiotherapy and Oncology*. 2021 Jul 1;160:159–65.
  - Bonvalot S, Rutkowski PL, Thariat J, Carrère S, Ducassou A, Sunyach MP, et al. NBTXR3, a first-in-class radioenhancer hafnium oxide nanoparticle, plus radiotherapy versus radiotherapy alone in patients with locally advanced soft-tissue sarcoma (Act.In.Sarc): a multicentre, phase 2–3, randomised, controlled trial. *Lancet Oncol*. 2019 Aug 1;20(8):1148–59.
  - Crapanzano R, Secchi V, Villa I. Co-Adjuvant Nanoparticles for Radiotherapy Treatments of Oncological Diseases. *Applied Sciences* 2021, Vol 11, Page 7073 [Internet]. 2021 Jul 30 [cited 2022 Mar 11];11(15):7073. Available from: <https://www.mdpi.com/2076-3417/11/15/7073/htm>
  - Li Y, Yun KH, Lee H, Goh SH, Suh YG, Choi Y. Porous platinum nanoparticles as a high-Z and oxygen generating nanozyme for enhanced radiotherapy in vivo. *Biomaterials*. 2019 Mar 1;197:12–9.
  - Mignot A, Truillet C, Lux F, Sancey L, Louis C, Denat F, et al. A top-down synthesis route to ultrasmall multifunctional Gd-based Silica nanoparticles for theranostic applications. *Chemistry - A European Journal* [Internet]. 2013

- May 3 [cited 2022 Mar 11];19(19):6122–36. Available from: <https://hal.archives-ouvertes.fr/hal-00828309>
14. Gharibshahi E, Saion E, Ashraf A, Gharibshahi L. Size-Controlled and Optical Properties of Platinum Nanoparticles by Gamma Radiolytic Synthesis. *Applied Radiation and Isotopes*. 2017 Dec 1;130:211–7.
  15. Zhang Y, Han X, Liu Y, Wang S, Han X, Cheng C. Research progress on nano-sensitizers for enhancing the effects of radiotherapy. *Cite this: Mater Adv*. 2022;2022:3709.
  16. Bao Z, He M, Quan H, Jiang D, Zheng Y, Qin W, et al. FePt nanoparticles: a novel nanoprobe for enhanced HeLa cells sensitivity to chemoradiotherapy. 2016; Available from: [www.rsc.org/advances](http://www.rsc.org/advances)
  17. Yang X, Salado-leza D, Porcel E, Vargas CRG, Savina F, Dragoe D, et al. A Facile One-Pot Synthesis of Versatile PEGylated Platinum Nanoflowers and Their Application in Radiation Therapy. *Int J Mol Sci* [Internet]. 2020 Mar 1 [cited 2022 Mar 11];21(5). Available from: [/pmc/articles/PMC7084439/](https://pubs-rsc-org.ezproxy.universite-paris-saclay.fr/en/content/articlehtml/2020/bm/c9bm02014d)
  18. Salado-Leza D, Porcel E, Yang X, Štefančíková L, Bolsa-Ferruz M, Savina F, et al. Green One-Step Synthesis of Medical Nanoagents for Advanced Radiation Therapy. *Nanotechnol Sci Appl* [Internet]. 2020 Aug 7 [cited 2022 Mar 11];13:61–76. Available from: <https://www.dovepress.com/green-one-step-synthesis-of-medical-nanoagents-for-advanced-radiation-peer-reviewed-fulltext-article-NSA>
  19. Li X, Porcel E, Menendez-Miranda M, Qiu J, Yang X, Serre C, et al. Highly Porous Hybrid Metal–Organic Nanoparticles Loaded with Gemcitabine Monophosphate: a Multimodal Approach to Improve Chemo- and Radiotherapy. *ChemMedChem*. 2020 Feb 5;15(3):274–83.
  20. Research, Center for Drug Evaluation and research F. Approval Letter for Radiogardase(Insoluble Prussian Blue) 21-626. 2003;
  21. Qin Z, Li Y, Gu N. Progress in Applications of Prussian Blue Nanoparticles in Biomedicine. Vol. 7, *Advanced Healthcare Materials*. Wiley-VCH Verlag; 2018.
  22. Ren C, Cheng Y, Li W, Liu P, Yang L, Lu Q, et al. Ultra-small Bi<sub>2</sub>S<sub>3</sub> nanodot-doped reversible Fe(II/III)-based hollow mesoporous Prussian blue nanocubes for amplified tumor oxidative stress-augmented photo-/radiotherapy. *Biomater Sci* [Internet]. 2020 Mar 31 [cited 2023 Apr 3];8(7):1981–95. Available from: <https://pubs-rsc-org.ezproxy.universite-paris-saclay.fr/en/content/articlehtml/2020/bm/c9bm02014d>
  23. Lin SY, Yao YQ, Zhang L, Feng JJ, Wang AJ. Cyanogel and its derived-materials: properties, preparation methods, and electrochemical applications. *Mater Today Energy*. 2021 Jun 1;20:100701.
  24. Liu ZY, Fu GT, Zhang L, Yang XY, Liu ZQ, Sun DM, et al. PdCo/Pd-Hexacyanocobaltate Hybrid Nanoflowers: Cyanogel-Bridged One-Pot Synthesis and Their Enhanced Catalytic Performance. *Scientific Reports* 2016 6:1 [Internet]. 2016 Aug 30 [cited 2022 May 13];6(1):1–10. Available from: <https://www-nature-com.ezproxy.universite-paris-saclay.fr/articles/srep32402>
  25. Paul G, Prado Y, Dia N, Rivière E, Laurent S, Roch M, et al. MnII-containing coordination nanoparticles as highly efficient T1contrast agents for magnetic resonance imaging. *Chemical Communications*. 2014;50(51):6740–3.
  26. Catala L, Mallah T. Nanoparticles of Prussian blue analogs and related coordination polymers: From information storage to biomedical

- applications. *Coord Chem Rev* [Internet]. 2017;346:32–61. Available from: <http://dx.doi.org/10.1016/j.ccr.2017.04.005>
27. Fornasieri G, Aouadi M, Delahaye E, Beaunier P, Durand D, Rivière E, et al. Elaboration of Prussian Blue Analogue/Silica Nanocomposites: Towards Tailor-Made Nano-Scale Electronic Devices. *Materials* 2012, Vol 5, Pages 385-403 [Internet]. 2012 Mar 5 [cited 2022 Oct 14];5(3):385–403. Available from: <https://www.mdpi.com/1996-1944/5/3/385/htm>
28. Fétiveau L, Paul G, Nicolas-Boluda A, Volatron J, George R, Laurent S, et al. Tailored ultra-small Prussian blue-based nanoparticles for MRI imaging and combined photothermal/photoacoustic theranostics. *Chemical Communications*. 2019;55(98):14844–7.
29. Biological evaluation of medical devices-16:45:28 MDT No reproduction or networking permitted without license from IHS COPYRIGHT PROTECTED DOCUMENT 16:45:28 MDT No reproduction or networking permitted without license from IHS. 2009;
30. Salado-Leza D, Traore A, Porcel E, Dragoe D, Muñoz A, Remita H, et al. Radio-Enhancing Properties of Bimetallic Au:Pt Nanoparticles: Experimental and Theoretical Evidence. [cited 2022 Oct 5]; Available from: [www.mdpi.com/journal/ijms](http://www.mdpi.com/journal/ijms)

- 1 Citations should appear here in the format A. Name, B. Name and C. Name, *Journal Title*, 2000, **35**, 3523; A. Name, B. Name and C. Name, *Journal Title*, 2000, **35**, 3523.

2 ...

We encourage the citation of primary research over review articles, where appropriate, in order to give credit to those who first reported a finding. [Find out more](#) about our commitments to the principles of San Francisco Declaration on Research Assessment (DORA).